

Research Paper

Experimental assessment of the energy performance of a renewable air-cooling unit based on a dew-point indirect evaporative cooler and a desiccant wheel

María Jesús Romero-Lara ^{a,*}, Francisco Comino ^b, Manuel Ruiz de Adana ^a^a Departamento de Química-Física y Termodinámica Aplicada, Escuela Politécnica Superior, Universidad de Córdoba, Campus de Rabanales, Antigua Carretera Nacional IV, km 396, 14071 Córdoba, España^b Departamento de Mecánica, Escuela Politécnica Superior, Universidad de Córdoba, Campus de Rabanales, Antigua Carretera Nacional IV, km 396, 14071 Córdoba, España

ARTICLE INFO

ABSTRACT

Keywords:

Advanced air-cooling system
Desiccant technology
Energy performance
Evaporative cooling
Experimental tests
Renewable energy source

Given the escalating energy consumption in cities worldwide, it is crucial to investigate the utilization of sustainable technologies and renewable energy sources. The number of empirical studies on the energy performance of hybrid air-cooling systems is limited. Therefore, the objective of this work is to experimentally study the energy performance of a novel renewable air-cooling unit. This prototype is mainly composed of a desiccant wheel and a dew-point indirect evaporative cooler to independently control the temperature, humidity, and carbon dioxide levels of indoor air. 64 experimental tests are carried out to fit an empirical model of this renewable air-cooling unit, focusing on outlet air conditions and the coefficient of performance. In addition, several performance indices are developed for desiccant wheel and dew-point indirect evaporative cooler: (i) moisture removal capacity; (ii) moisture removal capacity per unit of electrical power-consumption; (iii) dew-point efficiency and (iv) cooling capacity of dew-point indirect evaporative cooler per unit of electrical power-consumption. The highest values of dehumidification capacity, sensible cooling capacity and coefficient of performance for this renewable air-cooling unit are achieved for the most severe outdoor air conditions, namely $19.02 \text{ kg}\cdot\text{h}^{-1}$, 21.49 kW and 11.0, respectively. This work can serve as a reference for research on the feasibility of hybrid air-cooling systems in the scenarios of heat events and climate change world.

1. Introduction

Renewable energy sources and sustainable cooling technologies have become essential in addressing the escalating energy consumption in cities worldwide. The heating and cooling of buildings constitute 50 % of the overall energy consumption in the European Union. A significant percentage of this energy (70 %) is currently generated from fossil fuels [1]. An investigation across Europe showed that Mediterranean zone will suffer more than other European areas in the future due to global warming [2]. Moreover, the climate change scenario is giving rise to numerous challenges concerning also related human health [3]. One of the main effects of climate change is the increase in outside temperature around the world, which directly impacts demand for cooling energy. According to a research study, two advanced air-cooling systems showed an energy consumption three and four times lower than a traditional air-

cooling system under the Southern Europe climate conditions [4]. In a review work it was concluded that almost 60 % energy savings are achieved through the use of solar energy for the regeneration of a desiccant dehumidifier [5]. Therefore, there is a need to increase the number of experimental studies on renewable advanced air-cooling systems to obtain empirical models. This approach would enable a more accurate analysis of their real feasibility to buildings or renewable district networks. The majority of the hybrid air-cooling systems studied in the literature are based on integration with renewable energy sources. A desiccant air-cooling system achieved significant energy savings, up to 46.8 %, compared to a conventional air-cooling system [6]. Comparison between desiccant air-conditioning systems and evaporative cooling technology is also carried out in literature [7]. This technology is divided into direct evaporative coolers (DEC) and indirect evaporative coolers (IEC). The main difference between both evaporative cooling technologies lies in the direct or non-direct contact between the air flow

* Corresponding author.

E-mail address: p42rolam@uco.es (M.J. Romero-Lara).

Nomenclature	
Variables	
0	off
1	on, variable air flow rate
2	on, constant air flow rate
b	estimated parameter
BP	bypass air
CC	cooling coil
CO ₂	carbon dioxide
COP	coefficient of performance [-]
DF	DIEC fan
EER	energy efficiency ratio [-]
F	fan
FT	air filter
h	specific enthalpy [kJ·kg ⁻¹]
HC	heating coil
HCP	heating compensation percentage [%]
HP	hydraulic pump
KPI	key performance index
MAE	mean absolute error
MRC	moisture removal capacity [kg·h ⁻¹]
P	pressure drop [Pa]
PF	process fan of RACU
Q̄	thermal power [kW]
R	ratio [-]
R ²	coefficient of determination [-]
RH	relative humidity [%]
RF	regeneration fan of RACU
SH	steam humidifier
T	temperature [°C]
V̄	volumetric air flow [m ³ ·h ⁻¹]
VC	valve control
W̄	power consumption [kW]
X	input variable
Ȳ	estimated output variable
Acronyms	
AHU	air handling unit
DHCN	district heating and cooling network
DIEC	dew-point indirect evaporative cooler
DOE	design of experiments
DW	desiccant wheel
DX	direct expansion unit
ECM	electronically commutated motor
ePM	efficiency particulate matter
RACU	renewable air-cooling unit
Greek letters	
Σ	sum
ρ	air density [kg·m ⁻³]
Δ	increase
ε	efficiency [-]
ω	humidity ratio [g·kg ⁻¹]
Subscripts	
1 – 7	air states in RACU
aux,DW	auxiliar air state (T_2 , ω_1)
aux,RACU	auxiliar air state (T_1 , ω_3)
DIEC	dew-point indirect evaporative cooler
DF	DIEC fan
DP	dew-point
DW	desiccant wheel
e	exhaust
elect	electrical
HP	hydraulic pump
i	inlet
IDA	indoor air
L	latent
o	outlet
P	process
R	regeneration
RACU	renewable air-cooling unit
S	sensible
SP	set-point
T	total
U	useful
w	water

and water, respectively. Nevertheless, both DEC and IEC methods enable the temperature control of the supply air. A recent work indicated that the operation of a desiccant air-conditioning system was influenced by both ambient air temperature and humidity, with ambient air humidity being the decisive factor [8]. The coefficient of performance (COP) showed a strong correlation with the humidity ratio of the ambient air: the COP decreased nearly linearly as the humidity ratio increased. In another study on dew-point indirect evaporative cooler (DIEC) systems, it was also determined that the seasonal COP value was lower in climates zones characterised by high values of ambient humidity ratio [9]. The integration of DIEC systems with dehumidification systems could represent an interesting option in the context of applicability, reduction of carbon dioxide (CO₂) emissions and improvement of energy efficiency [10].

Desiccant systems based on desiccant wheels (DW) could be a potential alternative to conventional systems relying on direct compression (DX), in terms of moisture removal capacity (MRC) and energy consumption [11]. An experimental and numerical analysis of a DW was carried out in a work to determine its MRC [12]. The results showed that a effective control strategy for DW would allow controlling the removal of moisture, establishing the process air flow rate and the air regeneration temperature.

A study on hybrid desiccant cooling systems revealed that, in the

humid conditions of Taiwan, these systems can save between 7.7 % and 31.7 % more energy than traditional vapor compression systems during summer [13]. Another significant study experimentally investigated a solar desiccant cooling system, primarily consisting of a DW, an IEC, and a solar thermal system, which achieved a seasonal COP of 2.1 in the climates of Southern Europe [14]. Another research work evaluated the COP of a hybrid system featuring a DIEC and dehumidifying membranes [15], finding that the highest COP values, ranging from 4.5 to 9, occurred in the climate of Changsha between June and August.

Most studies in literature about hybrid air-cooling systems are based on energy simulations or mathematical models. Comprehensive annual simulation tools, such as EnergyPlus [16] and TRNSYS [17], are commonly used for these works. Nevertheless, it remains essential to conduct experimental studies on hybrid air-cooling systems to respond more reliably to the current situation of cooling energy demand. In a recent study, the results of a life cycle assessment of an experimental solar hybrid system exhibited more environmental benefits compared to a comercial DX system [18].

Given the global increase in outdoor air temperatures in recent years, the design and optimization of resilient air-cooling systems in extreme heat event scenarios is essential to achieving the Nearly Zero Energy Buildings (NZEB) goal. Implementing more sustainable air-cooling systems powered by renewable energy sources, as well as the renewable

energy storage, are among the advances to mitigate environmental impact [19]. According to these aspects and to address the research gap regarding empirical studies of hybrid air-cooling systems, this work experimentally studies the energy performance of an innovative renewable cooling desiccant technology. This renewable air-cooling unit (RACU) based on using a DW and a DIEC to control the humidity, temperature, and CO_2 levels of the air inside the building. An extensive range of experimental operating conditions is used to fit the empirical model of RACU in terms of outlet air conditions. Also, a detailed analysis of RACU components and RACU energy performance is performed.

2. Materials and methods

This section outlines the empirical methodology and experimental design employed in this study. It provides a detailed description of RACU, focusing on its main components and the design of its control strategy. Additionally, energy performance indicators are developed to analyse RACU and its main components.

2.1. Description of the renewable air-cooling unit

RACU is developed within the framework of a H2020 research project [20] to be integrated into renewable District Heating and Cooling Networks (DHCN). RACU is composed of two main technologies: a DIEC to control air temperature and a DW to control air humidity. RACU operated with two inlet air streams: process inlet (P_i) air and regeneration inlet (R_i) air to thermally activate the desiccant wheel. The process inlet air is divided into process outlet (P_o) air to supply cool air to the building and exhaust (e) air to exhaust moist air after the indirect evaporative cooling process, as shown in Fig. 1.

A nominal P_i air flow rate of $5236 \text{ m}^3 \cdot \text{h}^{-1}$ is considered to analyse the energy behaviour of the RACU system, where 55 % of this air flow rate, $2880 \text{ m}^3 \cdot \text{h}^{-1}$, is considered as cooled supply air and the remaining 45 % as exhaust moist air. One third of the nominal P_i air flow rate, $1745 \text{ m}^3 \cdot \text{h}^{-1}$, is established as nominal regeneration air flow rate. RACU is designed to be integrated with a DHCN. However, to perform a set of experimental tests, a natural gas boiler is used to supply a constant water temperature to the heating coil (HC) in RACU. The thermal consumption values are not included in the RACU performance indices, as this prototype is designed to leverage heat surpluses from DHCN. RACU operates without refrigerant gases are handled 100 % outdoor air.

2.1.1. Main components

RACU is composed of several elements to handle air, as observed from Fig. 1. The main characteristics of these components and the main operating principles are described in this section of the work.

The desiccant wheel is used to control the supply air humidity. This DW enabled a reduction in the humidity ratio of the process inlet air. The main technical characteristics of DW are summarised in Table 1.

The DW operated with two separate and opposing air streams. The DW has a 270° process circular sector and a 90° regeneration circular sector. The process air stream passed through the DW (state 1), reducing air humidity ratio, and increasing air temperature (state 2). An air bypass air (BP) is integrated into RACU. The BP is used when humidity control is not required (Fig. 1). On the other hand, the regeneration air stream (state 6) is used to remove moisture from the DW to the exhaust air (state 7). A picture and a schematic of the DW installed in the RACU prototype is shown in Fig. 2. A heating coil is used to thermally activate the DW of the RACU prototype. This HC is fed with hot water from a natural gas boiler. The standard operating conditions are inlet/outlet water temperature of $80/65^\circ\text{C}$ and water flow rate of 0.6 kg s^{-1} . The water flow rate to the HC is adjusted with a three-way valve with actuator (VC).

After passing through the DW, the process airflow is cooled with a dew-point indirect evaporative cooler. The technical characteristics of this DIEC are listed in Table 2.

DIEC is composed of a counterflow heat exchanger, which consisted of alternating wet and dry channels separated by thin plates. The primary air (process air) in DIEC is cooled along the dry channels without increase air moisture and subsequently supplied (state 3 in Fig. 1). Through the perforations located at the end of channels, 45 % of the primary air flow is recirculated through the adjacent wet channels. The remaining 55 % is cooled supplied air. Flowing in counter direction to

Table 1
Technical characteristics of DW.

Parameter	Value	Unit
Nominal dehumidification capacity	16	$\text{kg} \cdot \text{h}^{-1}$
Nominal process air flow rate	5236	$\text{m}^3 \cdot \text{h}^{-1}$
Nominal regeneration air flow rate	1745	$\text{m}^3 \cdot \text{h}^{-1}$
Rotor diameter	770	mm
Rotor thickness	200	mm
PF diameter	500	mm
PF nominal power	2.65	kW
RF diameter	280	mm
RF nominal power	1.00	kW
PF and RF motors	Variable speed ECM	
PF and RF electrical supply	400	V
Process circular sector	270	°
Regeneration circular sector	90	°
Desiccant material	Silica gel	—
Water vapour adsorption capacity	> 40	%

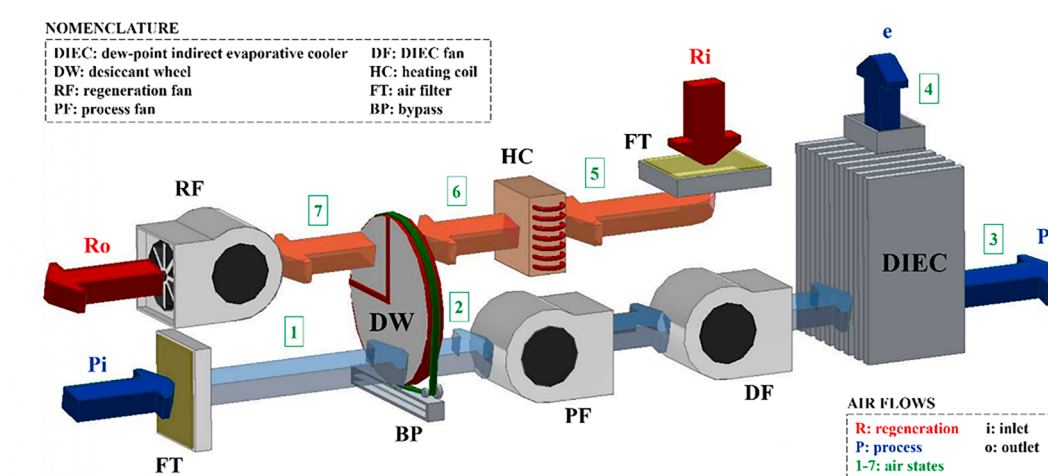


Fig. 1. Main components of the RACU system.

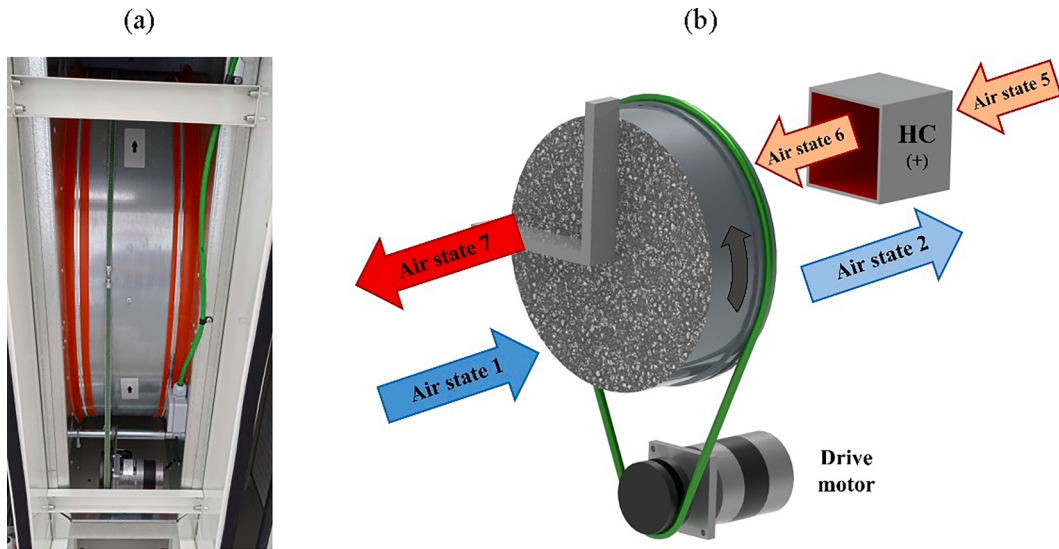


Fig. 2. Desiccant wheel installed in RACU: (a) picture and (b) operating principle.

Table 2
Technical characteristics of the DIEC.

Parameter	Value	Unit
Nominal cooling capacity	18	kW
Nominal supply air flow rate	2880	$\text{m}^3 \cdot \text{h}^{-1}$
Maximum external static pressure	230	Pa
DF diameter	560	mm
DF nominal power	1.5	kW
DF motor	Variable speed ECM	
DF electrical supply	380–415	V
Heat exchanger cores	2	—
Internal pumps	2	—
Water pump power	60	W
Water flow rate	13	$1 \cdot \text{min}^{-1}$
Chlorinators	1	—

the primary air in dry channels, the secondary air of wet channels is humidified and exhausted outside (state 4 in Fig. 1). The water flow rate to the DIEC is adjusted with a two-way valve (VC). More details of this DIEC configuration are explained in previous works [21]. A picture of DIEC and a schematic of its operating principle are shown in Fig. 3.

Other components as variable speed fans (F) and air filters (FT) are also integrated into the RACU prototype. A process fan (PF), a DIEC fan (DF) and a regeneration fan (RF) with a nominal inlet process air flow rate of $5236 \text{ m}^3 \cdot \text{h}^{-1}$ and a nominal inlet regeneration air flow rate of

$1745 \text{ m}^3 \cdot \text{h}^{-1}$ are included in Fig. 1. The system control of RACU allowed to modify these air flow rates values (Electronically Commutated Plug Fans). The three FT installed in RACU consist of one coarse filter (coarse 60 %) and two fine filters (ePM₁ 65 %) located at the inlet of the process air stream and at the inlet of the regeneration air stream, as observed from Fig. 1.

An image of the RACU prototype can be observed in Fig. 4. In this figure, the main air flows (process side in blue and regeneration side in red) are drawn on the prototype. A psychrometric diagram is also included where the different air conditions for an experimental test in RACU are represented. The process air side is defined by states 1 to 2, where the air humidity is decreased when passing through the DW; states 2 to 3, where the air temperature is decreased when passing through the DIEC, and states 2 to 4, where the air humidity is increased to exhaust it outside. The regeneration air side is defined by states 5 to 6, where the air temperature increased when passing through the HC, and by states 6 to 7, when the DW is thermally activated. Two auxiliary air states are also defined to obtain the value of several RACU performance indices: "aux,DW" as T_2 and w_1 air conditions and "aux,RACU" as T_1 and w_3 air conditions. Moreover, several images and technical characteristics of the HC and FT installed in RACU are shown in the Supplementary Material section of this work.

2.1.2. Control system and modes of operation

The combination of several elements in the RACU prototype is

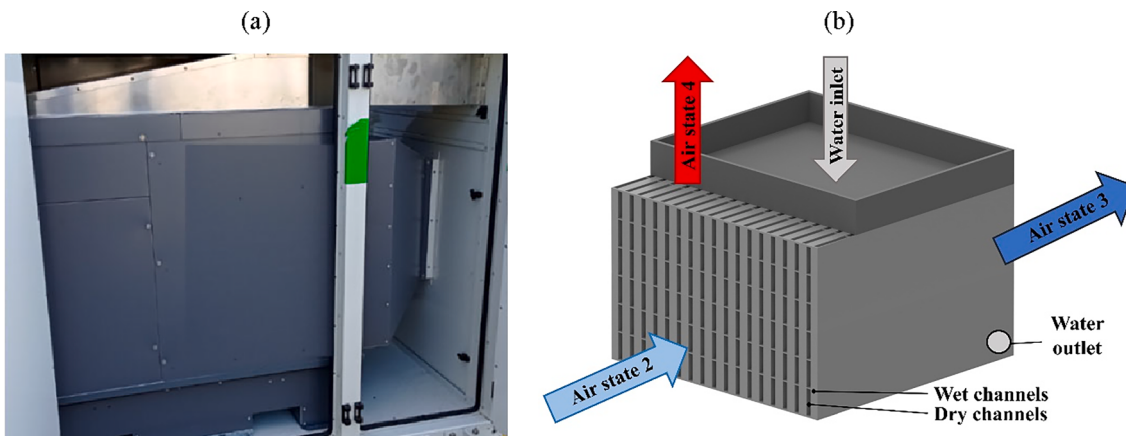


Fig. 3. Dew-point IEC installed in RACU: (a) picture and (b) operating principle.

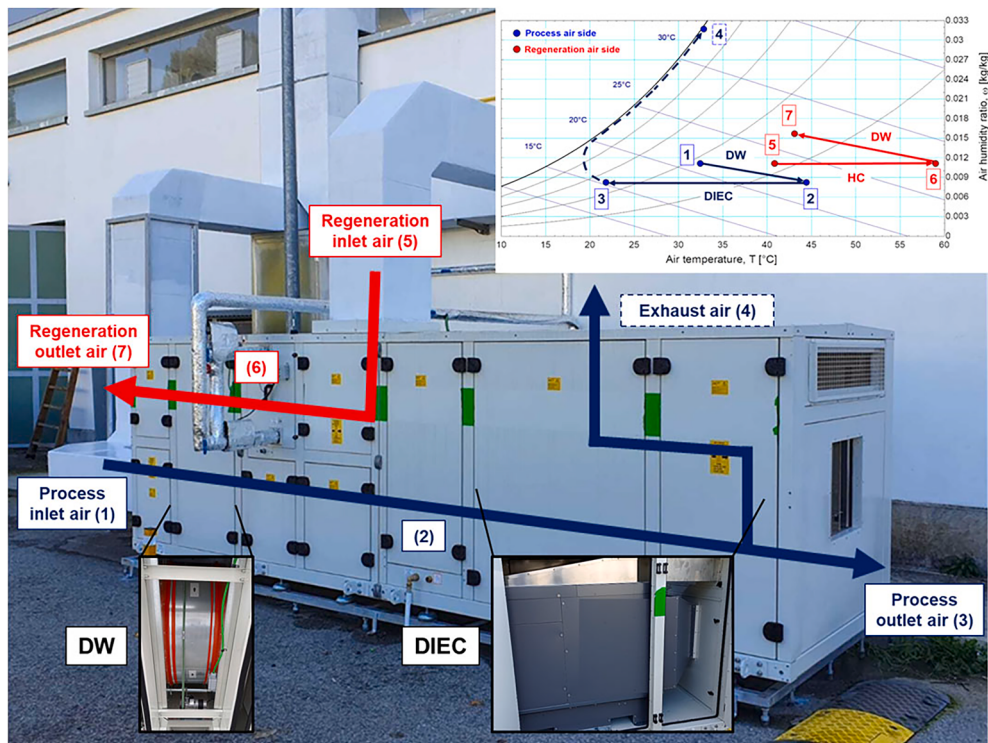


Fig. 4. Picture and air-cooling process of the RACU prototype.

designed to independently control the indoor air temperature (T_{IDA}), indoor air humidity (ω_{IDA}), and indoor air CO_2 concentration ($CO_{2,IDA}$). An occupied room is not included in this study. Hence, the conditions of the process outlet air (state 3 in Fig. 1) are considered as the supply air conditions. RACU included a control system based on three independent main control loops. The first one is a temperature control loop (T), the second one is a humidity control loop (H) and the third one is a ventilation control loop (V), as shown in Fig. 5. Each control loop is divided into two specific modes of operation: 1 when it is activated and 0 when it is not activated. In addition, operating mode 2 is included to indicate

operation of RACU at a constant airflow during the experimental tests for this work. These experimental tests based on the statistical technique of 'Design of Experiments' (DOE) imposed certain P_i and R_i air flow rates. The process inlet and regeneration air conditions are adjusted with a process air handling unit (AHU_p) and a regeneration air handling unit (AHU_r). The control system checks the T_{IDA} , ω_{IDA} and $CO_{2,IDA}$ values, and then it executes the control actions, to reach the set-point (SP) conditions. These set-points conditions can be modified through a display installed in the electrical panel. This control strategy is established according to the increase (Δ) of temperature (ΔT), humidity ratio

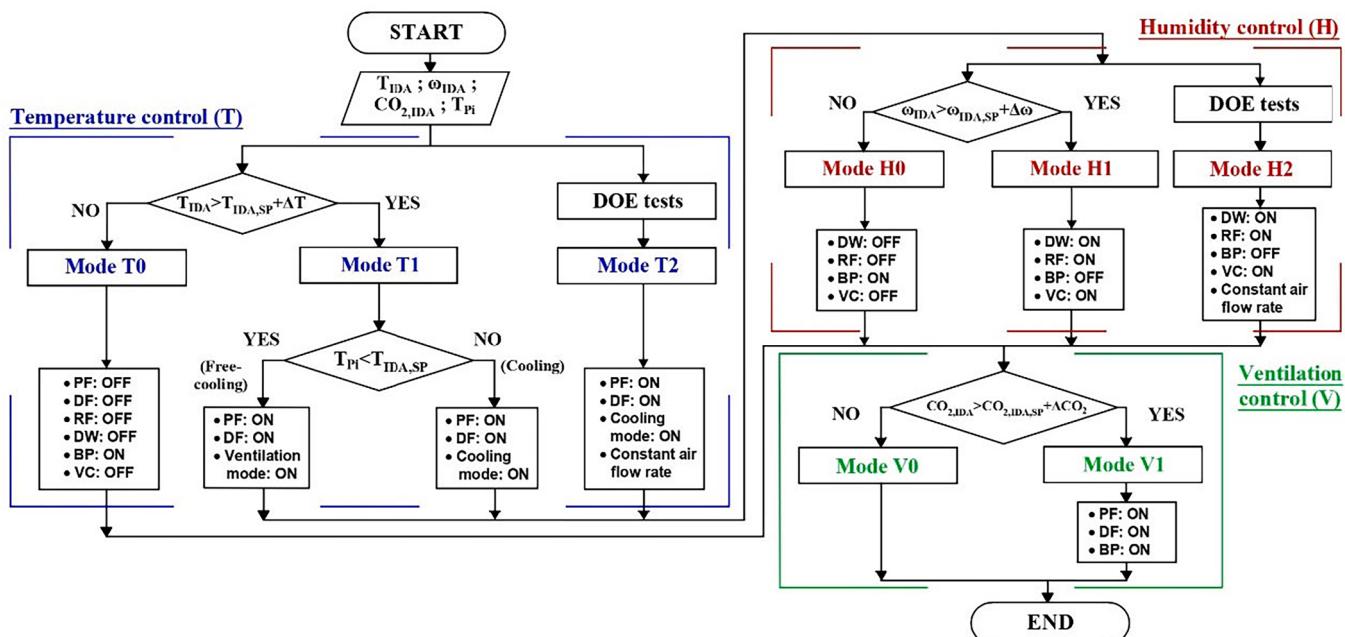


Fig. 5. RACU control logic diagram.

($\Delta\omega$) and CO_2 concentration (ΔCO_2), as shown in Fig. 5. These increases correspond to the difference between the IDA conditions and set-point conditions established inside the room (T , ω , CO_2).

According to the combination of the three control loops, seven operating modes are established for RACU:

- Air temperature control (T1H0V0). It consisted of reducing the IDA temperature. Depending on the T_{pi} value, the free-cooling or cooling mode is activated. In this case, dehumidification and ventilation modes are off.
- Air temperature control and air humidity control (T1H1V0). This mode is activated when it is necessary to reduce the T_{IDA} and ω_{IDA} values. Therefore, the components PF, RF, DF and DW are operating.
- Constant air flow rate (T2H2V0). This mode is activated for the experimental tests of this work. For these tests N1-N64, RACU operated with a constant air flow rate.
- Air temperature control and ventilation control (T1H0V1). It turned on when the T_{IDA} and $CO_{2,IDA}$ values are higher than their respective set-points values.
- Air temperature control, air humidity control and ventilation control (T1H1V1). It consisted of reducing the values of T_{IDA} , ω_{IDA} and $CO_{2,IDA}$, since they are higher than the $T_{IDA,SP}$, $\omega_{IDA,SP}$ and $CO_{2,IDA,SP}$ values, respectively. In this mode, all components of the RACU prototype are operating.
- Ventilation control (TOH0V1). It is activated to adjust the air flow rate of the process fan with the aim of reducing the $CO_{2,IDA}$ value and improve indoor air quality.
- RACU off (TOH0V0). According to the indoor air conditions (T_{IDA} , ω_{IDA} and $CO_{2,IDA}$) the operation of RACU is not necessary.

For all these modes of operation, both process and regeneration volumetric airflows of the RACU prototype is adjusted from 20 % to 100 % of their respective nominal values, as shown in Fig. 6. RACU operated at 100 % of its nominal airflow rate when ΔT , $\Delta\omega$ and ΔCO_2 are equal to 2 °C, 2 g·kg⁻¹ and 500 ppm, respectively. When all set-point conditions are reached, the percentage of these volumetric airflows is maintained at 20 % to provide a minimum ventilation airflow rate (Fig. 6). In the present work, to analyse the experimental behaviour of the RACU prototype, constant air flow rates are used (Fig. 6).

2.2. Experimental setup

An experimental facility is designed and built to study the thermal behaviour of the RACU prototype under different operating conditions. The values of inlet air temperature, inlet air humidity ratio, and inlet volumetric air flow of the process and regeneration streams are adjusted for each experimental test by using two air handling units, see AHU_P and AHU_R in Fig. 7. The main characteristics of each AHU can be observed in the Supplementary Material section. Instrumentation such as sensors for air temperature (T), air relative humidity (RH), air CO_2 concentration (CO_2), water temperature (T_W), air pressure drop (P), volumetric water flow (\dot{V}) and electrical-power consumption (\dot{W}) are also used to measure each air state (1 to 7), as shown in Fig. 7. Before testing, calibration of T sensors was carried out using the Scan-Sense TC15M calibrator, with a range of -40 °C to 150 °C. Calibration of humidity sensors was obtained using mainly four different salts, a base plate and a measuring cup. The type and accuracy of all sensors used in this work are listed in Table 3.

2.3. Design of experiments

A complete set of experimental tests (N1-N64) under different operating conditions are carried out to analyse the energy performance of RACU and to obtain a complete empirical model. This set of experimental tests is based on DOE, specifically the Box-Behnken design [22]. The design consisted of 64 experimental tests with 8 central points. The input variables for these experimental tests are process inlet air temperature (T_{Pi}), process inlet air humidity ratio (ω_{Pi}), process inlet volumetric air flow (\dot{V}_{Pi}), regeneration inlet air temperature (T_{Ri}), regeneration inlet air humidity ratio (ω_{Ri}), regeneration inlet volumetric air flow (\dot{V}_{Ri}), and exhaust air ratio (R_e). This ratio is defined as the relationship between the exhaust air volumetric flow rate (\dot{V}_e) and \dot{V}_{Pi} , as shown in Eq. (1). The values established for these input parameters for this study are shown in Table 4.

$$R_e = \frac{\dot{V}_e}{\dot{V}_{Pi}} \quad (1)$$

On the other hand, the response variables are process outlet air temperature (T_{Po}), process outlet air humidity ratio (ω_{Po}), regeneration outlet air temperature (T_{Ro}), regeneration outlet air humidity ratio (ω_{Ro}), and electrical-power consumption (\dot{W}_{elect}) of the RACU prototype.

The set of operating conditions for each experimental test is listed in

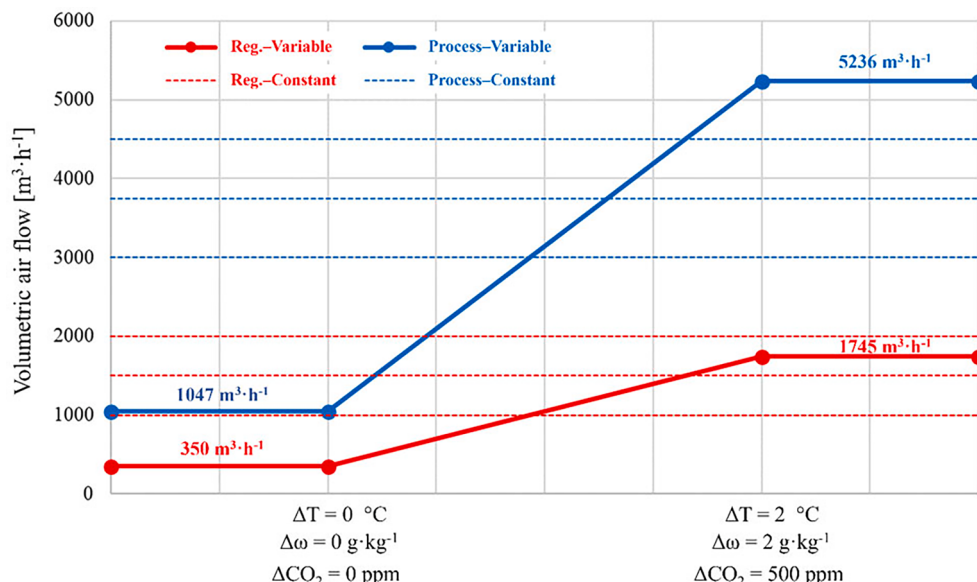


Fig. 6. Volumetric air flow rates control for the RACU prototype.

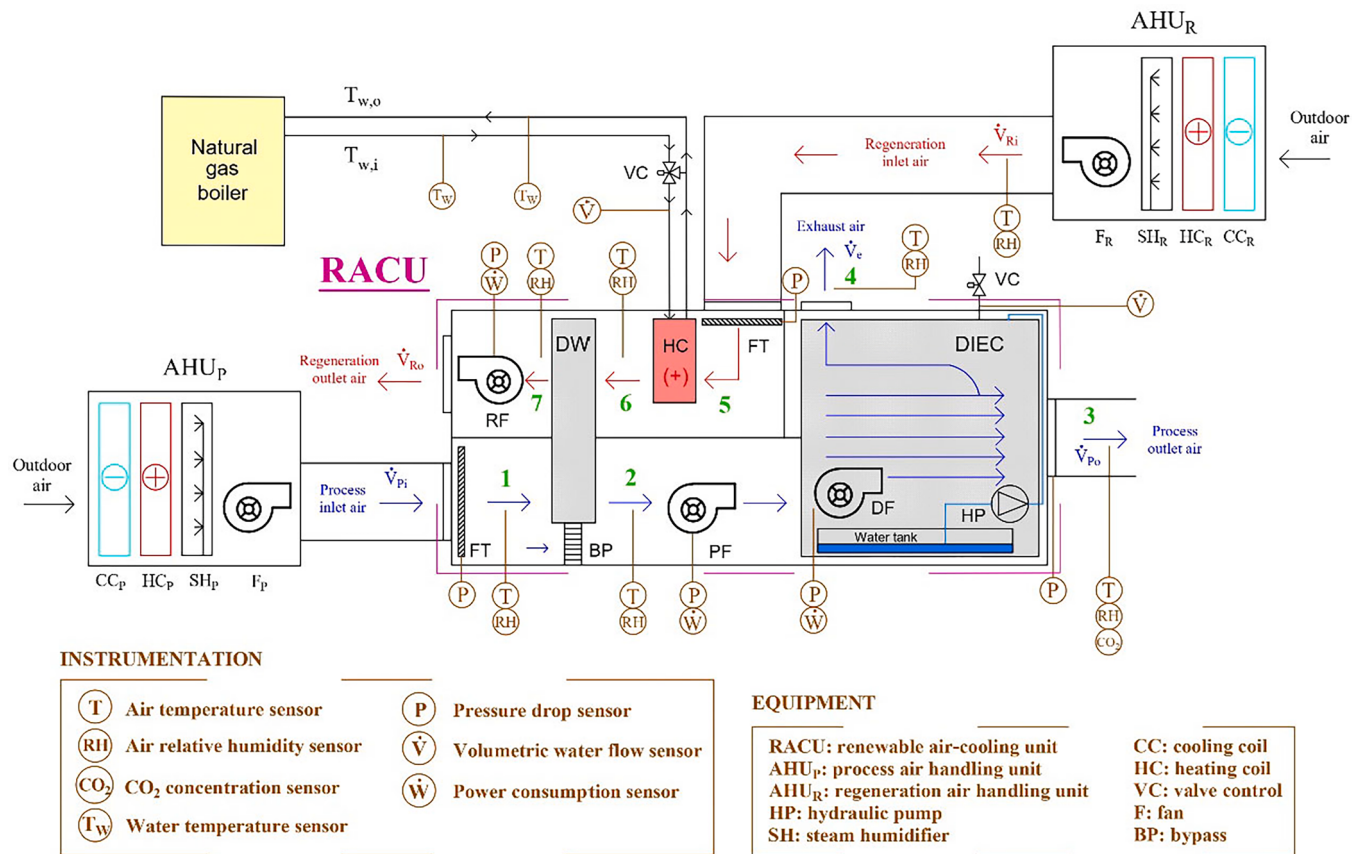


Fig. 7. Experimental setup and instrumentation at RACU.

Table 3
Types and accuracy of sensors used in the experimental setup.

Variable	Type	Measurement range	Accuracy
T	NTC	0–80 [°C]	±0.5 [°C]
RH	Capacitive	0–95 [%]	±3.0 [%]
CO ₂	Non-Dispersive Infrared detector	0–2000 [ppm]	±5.0 % reading
T _w	NTC	0–150 [°C]	±0.5 [°C]
P	Differential pressure transmitter	50–500 [Pa]	±6.0 % reading
̇V	Ultrasonic water flow rate transmitter	0–1.38 [l·s ⁻¹]	±1.2 % reading
̇W	Three-phase power sensor	0.01–9.99 [kW]	±1.0 % reading

Table 4
Established ranges for DOE input variables for the RACU prototype.

Input parameter	Air state	Values	Unit
Process inlet air temperature, T _{Pi}	1	24–32–40	°C
Process inlet air humidity ratio, ω _{Pi}	1	8–11–14	g·kg ⁻¹
Process inlet volumetric air flow, ̇V _{Pi}	1	3000–3750–4500	m ³ ·h ⁻¹
Regeneration inlet air temperature, T _{Ri}	5	24–32–40	°C
Regeneration inlet air humidity ratio, ω _{Ri}	5	8–11–14	g·kg ⁻¹
Regeneration inlet volumetric air flow, ̇V _{Ri}	5	1000–1500–2000	m ³ ·h ⁻¹
Exhaust air ratio, R _e	4/1	0.3–0.5–0.7	—

Table 5. These 64 tests are ordered from lowest to highest value of process outlet volumetric air flow (\dot{V}_{Po}). These \dot{V}_{Po} values are measured with an anemometer and verified according to the expression in Eq. (1). All the experimental tests indicated in Table 5 are carried out during a steady-state period of 30 min. For each test, the values of the response variables are obtained as the average value of these variables measured during the period of 30 min.

2.4. Performance of desiccant wheel and dew-point indirect evaporative cooler

In this work, the performance of the DW and DIEC components integrated into RACU is evaluated using several performance indices. The MRC and MRC per electrical power consumed by the process and regeneration fans (KPI_{DW}) are calculated for the DW, as shown in Eq. (2) and Eq. (3), respectively. For the DIEC, the dew-point efficiency (ϵ_{DP}) is determined for each experimental test according to Eq. (4). The useful sensible cooling capacity of DIEC ($\dot{Q}_{S,DIEC,U}$) is calculated according to the difference in air conditions between states 2 and 3 in RACU, combined with the \dot{V}_{Po} value for each test, as described in Eq. (5). Additionally, KPI_{DIEC} , indicating the $\dot{Q}_{S,DIEC,U}$ per unit of DIEC fan electrical power-consumption, is also determined according to Eq. (5). The DIEC system's role in offsetting the sensible heat generated by the DW is quantified by the Heating Compensation Percentage (HCP), calculated for each test as the percentage of the total sensible cooling capacity of the DIEC ($\dot{Q}_{S,DIEC,T}$) utilized to compensate for the sensible heating produced by the DW ($\dot{Q}_{S,DW}$), see Eq. (6).

$$MRC = \rho_1 \cdot \dot{V}_{Pi} \cdot (\omega_1 - \omega_2) \quad (2)$$

Table 5

Summary of experimental tests conditions to obtain the RACU empirical model.

Test	T_{Pi}	ω_{Pi}	\dot{V}_{Pi}	T_{Ri}	ω_{Ri}	\dot{V}_{Ri}	R_e	\dot{V}_{Po}
	[°C]	[g·kg ⁻¹]	[m ³ ·h ⁻¹]	[°C]	[g·kg ⁻¹]	[m ³ ·h ⁻¹]	[-]	[m ³ ·h ⁻¹]
N1	32	11	3000	24	11	1500	0.7	900
N2	32	11	3000	40	11	1500	0.7	900
N3	24	11	3750	32	11	1000	0.7	1125
N4	40	11	3750	32	11	1000	0.7	1125
N5	24	11	3750	32	11	2000	0.7	1125
N6	40	11	3750	32	11	2000	0.7	1125
N7	32	8	3750	32	8	1500	0.7	1125
N8	32	14	3750	32	8	1500	0.7	1125
N9	32	8	3750	32	14	1500	0.7	1125
N10	32	14	3750	32	14	1500	0.7	1125
N11	32	11	4500	24	11	1500	0.7	1350
N12	32	11	4500	40	11	1500	0.7	1350
N13	24	11	3000	32	8	1500	0.5	1500
N14	40	11	3000	32	8	1500	0.5	1500
N15	24	11	3000	32	14	1500	0.5	1500
N16	40	11	3000	32	14	1500	0.5	1500
N17	32	8	3000	32	11	1000	0.5	1500
N18	32	14	3000	32	11	1000	0.5	1500
N19	32	8	3000	32	11	2000	0.5	1500
N20	32	14	3000	32	11	2000	0.5	1500
N21 ^a	32	11	3750	32	11	1500	0.5	1875
N22 ^a	32	11	3750	32	11	1500	0.5	1875
N23 ^a	32	11	3750	32	11	1500	0.5	1875
N24 ^a	32	11	3750	32	11	1500	0.5	1875
N25 ^a	32	11	3750	32	11	1500	0.5	1875
N26 ^a	32	11	3750	32	11	1500	0.5	1875
N27 ^a	32	11	3750	32	11	1500	0.5	1875
N28 ^a	32	11	3750	32	11	1500	0.5	1875
N29	32	11	3750	24	8	1000	0.5	1875
N30	32	11	3750	40	8	1000	0.5	1875
N31	32	11	3750	24	14	1000	0.5	1875
N32	32	11	3750	40	14	1000	0.5	1875
N33	32	11	3750	24	8	2000	0.5	1875
N34	32	11	3750	40	8	2000	0.5	1875
N35	32	11	3750	24	14	2000	0.5	1875
N36	32	11	3750	40	14	2000	0.5	1875
N37	24	8	3750	24	11	1500	0.5	1875
N38	40	8	3750	24	11	1500	0.5	1875
N39	24	14	3750	24	11	1500	0.5	1875
N40	40	14	3750	24	11	1500	0.5	1875
N41	24	8	3750	40	11	1500	0.5	1875
N42	40	8	3750	40	11	1500	0.5	1875
N43	24	14	3750	40	11	1500	0.5	1875
N44	40	14	3750	40	11	1500	0.5	1875
N45	32	11	3000	24	11	1500	0.3	2100
N46	32	11	3000	40	11	1500	0.3	2100
N47	24	11	4500	32	8	1500	0.5	2250
N48	40	11	4500	32	8	1500	0.5	2250
N49	24	11	4500	32	14	1500	0.5	2250
N50	40	11	4500	32	14	1500	0.5	2250
N51	32	8	4500	32	11	1000	0.5	2250
N52	32	14	4500	32	11	1000	0.5	2250
N53	32	8	4500	32	11	2000	0.5	2250
N54	32	14	4500	32	11	2000	0.5	2250
N55	24	11	3750	32	11	1000	0.3	2625
N56	40	11	3750	32	11	1000	0.3	2625
N57	24	11	3750	32	11	2000	0.3	2625
N58	40	11	3750	32	11	2000	0.3	2625
N59	32	8	3750	32	8	1500	0.3	2625
N60	32	14	3750	32	8	1500	0.3	2625
N61	32	8	3750	32	14	1500	0.3	2625
N62	32	14	3750	32	14	1500	0.3	2625
N63	32	11	4500	24	11	1500	0.3	3150
N64	32	11	4500	40	11	1500	0.3	3150

^a Tests N21-N28 are central points of the design of experiments.

$$KPI_{DW} = \frac{MRC}{|\dot{W}_{PF}| + |\dot{W}_{RF}|} \quad (3)$$

$$\varepsilon_{DP} = \frac{T_2 - T_3}{T_2 - T_{DP,2}} \quad (4)$$

$$KPI_{DIEC} = \frac{|\dot{Q}_{S,DIEC,U}|}{|\dot{W}_{DF}|} = \frac{\rho_3 \cdot \dot{V}_{Po} \cdot |(h_3 - h_2)|}{|\dot{W}_{DF}|} \quad (5)$$

$$HCP = \frac{\dot{Q}_{S,DW}}{|\dot{Q}_{S,DIEC,T}|} \cdot 100 = \frac{\rho_1 \cdot \dot{V}_{Pi} \cdot (h_{aux,DW} - h_1)}{\rho_2 \cdot \dot{V}_{Pi} \cdot |(h_3 - h_2)|} \cdot 100 \quad (6)$$

Where ρ is the air density and \dot{W}_{PF} , \dot{W}_{RF} and \dot{W}_{DF} are the electrical power consumed by the PF, RF and DIEC fan, respectively. The state 1 (process inlet air to DW), state 2 (process inlet air to DIEC), state 3 (process outlet air from DIEC) and state 4 (wet exhaust air from DIEC) can be observed in Fig. 1. As indicated previously, two auxiliary air states ("aux,DW" and "aux,RACU") are defined to obtain the value of several performance indices.

2.5. Energy performance of renewable air-cooling unit

The energy performance index of the RACU prototype, which integrated its sensible and latent capacity, is also evaluated for each experimental test. The fit of this index and the output parameters for RACU is carried out using the Statgraphics software [23].

The COP for RACU is calculated according to the values of the sensible cooling capacity of RACU ($\dot{Q}_{S,RACU}$), latent capacity of RACU ($\dot{Q}_{L,RACU}$) and total \dot{W}_{elect} for each test shown in Table 5. The expressions to obtain the $\dot{Q}_{S,RACU}$ and $\dot{Q}_{L,RACU}$ values are indicated in Eq. (7) and Eq. (8), respectively.

$$|\dot{Q}_{S,RACU}| = \rho_3 \cdot \dot{V}_{Po} \cdot |(h_3 - h_{aux,RACU})| \quad (7)$$

$$|\dot{Q}_{L,RACU}| = \rho_3 \cdot \dot{V}_{Po} \cdot |(h_{aux,RACU} - h_1)| \quad (8)$$

The value of \dot{W}_{elect} for RACU is obtained for each experimental test as the sum of the electrical-power consumed by the PF, RF, DF, the drive motor of DW and the internal hydraulic pump in DIEC, as shown in Eq. (9).

$$\dot{W}_{elect} = \dot{W}_{PF} + \dot{W}_{RF} + \dot{W}_{DF} + \dot{W}_{motor,DW} + \dot{W}_{HP,DIEC} \quad (9)$$

The COP values for the RACU prototype are obtained for each experimental test, according to the respective sensible cooling capacity and latent capacity of RACU, as shown in Eq. (10).

$$COP = \frac{|\dot{Q}_{S,RACU}| + |\dot{Q}_{L,RACU}|}{|\dot{W}_{elect}|} \quad (10)$$

The Box-Behnken design adopted for this work is an experimental design based on the response surface methodology. The effect of 7 input variables on 5 output variables is studied through 64 different experimental tests at RACU, with the objective of achieving high values of coefficient of determination (R^2). Second order polynomial equations are used to obtain the relationship between the input and output parameters. This polynomial model is expressed by Eq. (11), where \hat{Y} is the estimated output value (T_{Po} , ω_{Po} , T_{Ro} , ω_{Ro} and \dot{W}_{elect}), X are the input parameters (T_{Pi} , ω_{Pi} , \dot{V}_{Pi} , T_{Ri} , ω_{Ri} , \dot{V}_{Ri} and R_e); b_0 is the average response in each model, and b_b , b_{ii} and b_{ij} are the estimated parameters of the linear, quadratic, and second-order terms, respectively. Therefore, 5 regression equations are fitted to the experimental data for the present work.

$$\hat{Y} = b_0 + \sum_{i=1}^k b_i \cdot X_i + \sum_{i=1}^k b_{ii} \cdot X_i^2 + \sum_{i=1}^{k-1} \sum_{i=2j>i}^k b_{ij} \cdot X_i \cdot X_j \quad (11)$$

3. Results and analysis

The experimental results of two case studies are presented in this section. In the first case study, the main operation modes, and the thermal behaviour of the RACU prototype are analysed under real outdoor conditions in Cordoba (Spain). In the second case study, the energy performance of DW, DIEC and RACU are shown and analysed under different laboratory conditions.

3.1. Case study 1: Daily performance under real outdoor conditions

The RACU prototype is designed to independently control T_{IDA} , ω_{IDA} and $CO_{2,IDA}$, as shown in Fig. 5. In this work, a real case of the daily energy performance of RACU under real outdoor conditions is shown, without application to a building, to verify the developed control strategy, as observed from Fig. 8. AHUp and AHUR were not connected in this case study. Hence, the input variables and output variables for RACU are analysed. The inlet air conditions (T_{Pi} and ω_{Pi}) corresponded to the outdoor air conditions of Cordoba, Spain, on July 13, 2023. The main operating modes of RACU were adjusted for the $T_{Po,SP}$ value of 16 °C and the $\omega_{Po,SP}$ value of 6 g·kg⁻¹ (Fig. 8). The operating modes of RACU for this demonstrative case are also shown in Fig. 8. On that day, the T_{Pi} values exhibited a gradual increase, starting at 26.1 °C and reaching 42.5 °C. However, due to the established $T_{Po,SP}$, the T_{Po} values were between 16 °C and 18 °C. Meanwhile, the ω_{Pi} values remained within the range of 7.41 g·kg⁻¹ to 9.85 g·kg⁻¹. However, due to the established $\omega_{Po,SP}$, the ω_{Po} values were between 6 g·kg⁻¹ and 8 g·kg⁻¹, as observed from Fig. 8. RACU was operational during office hours, from 9:30 a.m. to 6:30p.m. The average T_{Pi} value and the average ω_{Pi} value were 35.9 °C and 8.7 g·kg⁻¹, respectively. The seasonal COP for RACU during this day in Cordoba had a high value, 14.0. The main operating modes activated during that period were T1H1V0 (66.4 %), T0H0V1 (17.2 %), and T1H0V0 (16.11 %) such as shown in Fig. 8, due to the outdoor air conditions and variable control capacity for this real case study.

The T1H1V0 mode was activated when the values of T_{Pi} and ω_{Pi} are above the values of T_{SP} and ω_{SP} . This situation occurred mainly between 11:50 a.m. and 12:30p.m. and from 5:00p.m., when the outdoor air conditions are more severe (Fig. 8). The T_{Pi} values between 11:50 a.m. and 12:30p.m. are around 35 °C, so RACU managed to reduce the Pi air by 19 °C. RACU also achieved the reduction of 3.50 g·kg⁻¹ of the ω_{Pi} values during that same period (Fig. 8). The T_{Po} values from 5:00p.m are around 18 °C due to the highest T_{Pi} values (42.5 °C) and the consequent higher \dot{V}_{Pi} values, between 3000 m³·h⁻¹ and 5300 m³·h⁻¹. On the other hand, the T0H0V1 mode was activated when the T_{Pi} and ω_{Pi} values reached the T_{SP} and ω_{SP} values. However, the RACU system still operating in ventilation mode, as observed from Fig. 8. With Case study 1, the variable air flow control of RACU according to the ΔT , $\Delta \omega$ and ΔCO_2 values can be verified, as can be observed in Fig. 6.

3.2. Case study 2: Performance under experimental test conditions

An empirical model of the RACU prototype is adjusted and validated in this section. The values and uncertainties for each parameter obtained are shown in the Supplementary Material section. The uncertainty is determined according to the accuracy values of all the sensors used in this work and following the 'Guide to the expression of Uncertainty in Measurement' (GUM) [24].

3.2.1. Analysis of process outlet air conditions

The T_{Po} and ω_{Po} values are obtained for all experimental tests performed on the RACU prototype, as indicated in Table 5. The T_{Po} and ω_{Po} results for tests N1-N64 are depicted in the psychrometric chart of Fig. 9. Several shapes (square, circle, cross, asterisk, etc.) in Fig. 9 represent different inlet air conditions (T_{Pi} and ω_{Pi}). Different colours are also used to represent different \dot{V}_{Po} values, as illustrated in Fig. 9. The range of the results of T_{Po} and ω_{Po} are from 13.9 °C to 26.3 °C and from 5.35 g·kg⁻¹ to 11.26 g·kg⁻¹, respectively. The lowest T_{Po} value (13.9 °C) is achieved under the operating conditions of test N7, with the T_{Pi} value of 32 °C, the ω_{Pi} value of 8 g·kg⁻¹ and the \dot{V}_{Po} value of 1125 m³·h⁻¹. However, the highest T_{Po} value (26.3 °C) is obtained for test N56, with the T_{Pi} value of 40 °C, the ω_{Pi} value of 11 g·kg⁻¹ and the \dot{V}_{Po} value of 2625 m³·h⁻¹. Therefore, higher T_{Po} values are observed due to the increase of T_{Pi} , ω_{Pi} and \dot{V}_{Po} values (Fig. 9). The \dot{V}_{Po} value in test N7 is 42.8 % of the \dot{V}_{Po}

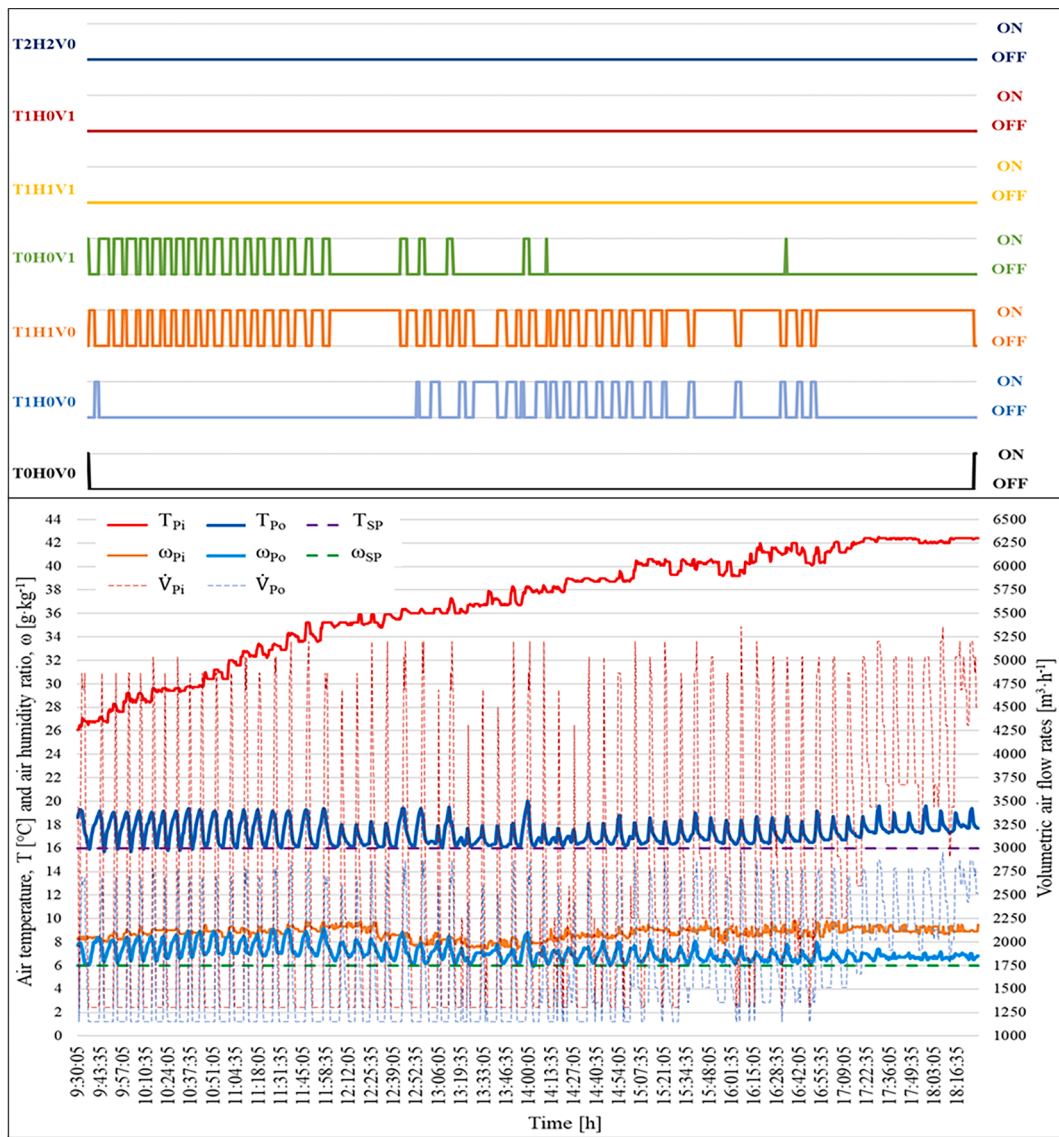


Fig. 8. Operating modes of RACU in a real case (Cordoba, Spain, 13th July 2023).

value in test N56, see Table 5. The lowest ω_{Po} value ($5.35 \text{ g}\cdot\text{kg}^{-1}$) is achieved under the test N41 operating conditions, with the minimum values of T_{Pi} and ω_{Pi} , 24°C and $8 \text{ g}\cdot\text{kg}^{-1}$, respectively. Nevertheless, the highest ω_{Po} value ($11.26 \text{ g}\cdot\text{kg}^{-1}$) is shown for the test N44, with the maximum values of T_{Pi} and ω_{Pi} , 40°C and $14 \text{ g}\cdot\text{kg}^{-1}$, respectively. Higher values of ω_{Po} are observed due to the increase of T_{Pi} and ω_{Pi} values. \dot{V}_{Po} had the same value for both experimental tests N41 and N44 ($1875 \text{ m}^3\cdot\text{h}^{-1}$), see Table 5. An increase in T_{Po} values is also appreciated in this case, 14.9°C for test N41 and 25.2°C for test N44. Another comparative analysis is performed between tests N1 and N64. They showed the same T_{Pi} value (32°C) and ω_{Pi} value ($11 \text{ g}\cdot\text{kg}^{-1}$) but different \dot{V}_{Po} values, 900 and $3150 \text{ m}^3\cdot\text{h}^{-1}$, respectively. An increase of 8.7°C and $2.23 \text{ g}\cdot\text{kg}^{-1}$ is observed in T_{Po} and ω_{Po} values between the experimental tests N1 and N64 due to the increase of \dot{V}_{Po} value. Thus, the lowest values of process outlet air conditions are achieved under the lowest \dot{V}_{Po} values, as observed from Fig. 9.

3.2.2. Adjustment and validation of the empirical model for the prototype

An empirical model of the RACU prototype is adjusted in terms of process outlet air conditions (T_{Po} and ω_{Po}), regeneration outlet air conditions (T_{Ro} and ω_{Ro}) and COP. The values of the estimated parameters for each output variable are shown in Table 6.

R^2 and several statistical indices for the T_{Po} , ω_{Po} , T_{Ro} , ω_{Ro} and COP empirical models are also shown in Table 6. R^2 values in good agreement, above 0.94 except ω_{Ro} , are achieved for the extensive number of experimental tests that are carried out in this work (N1–N64). The highest accuracy value is displayed by the COP model, which is 0.9804. Low values of deviation are also obtained for all these empirical models, between 0.0407 for ω_{Po} and 0.5817 for ω_{Ro} , see Table 6.

The results obtained from the experimental tests and the results obtained from these polynomial models are used for validation of the T_{Po} , ω_{Po} , T_{Ro} and ω_{Ro} empirical models (Fig. 10). The deviations between experimental and numerical results for T_{Po} ($\pm 0.51^\circ\text{C}$) and ω_{Po} ($\pm 0.04 \text{ g}\cdot\text{kg}^{-1}$) are shown in Fig. 10a and Fig. 10b, respectively. According to the regeneration air side, the deviations between experimental and numerical results of T_{Ro} (Fig. 10c) and experimental and numerical results of ω_{Ro} (Fig. 10d) are also low. Thus, the second-order approach adopted in the RACU model can be assumed to be valid for the output variables T_{Po} , ω_{Po} , T_{Ro} and ω_{Ro} .

3.2.3. Performance analysis of desiccant wheel and dew-point indirect evaporative cooler

The DW performance results in terms of MRC and KPI_{DW} are obtained for all experimental tests carried out at RACU, see values in Fig. 11.

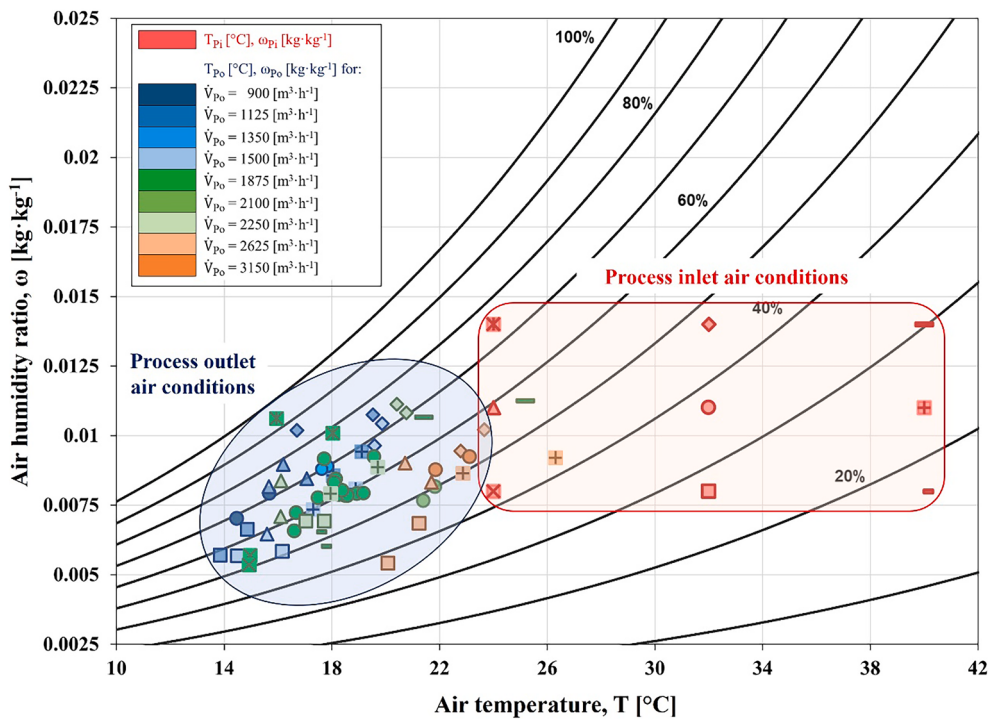


Fig. 9. Experimental results of process outlet air conditions for the tests N1–N64.

According to the expression of Eq. (2), the range of the *MRC* values is between $6.26 \text{ kg} \cdot \text{h}^{-1}$ and $19.02 \text{ kg} \cdot \text{h}^{-1}$ (Fig. 11). The lowest *MRC* value ($6.26 \text{ kg} \cdot \text{h}^{-1}$) is shown for test N61, in which the ω_1 value is $8 \text{ g} \cdot \text{kg}^{-1}$ and the T_1 value is 32°C . However, the highest *MRC* value ($19.02 \text{ kg} \cdot \text{h}^{-1}$) is shown for test N47, in which the ω_1 value is $11 \text{ g} \cdot \text{kg}^{-1}$ and the T_1 value is 24°C . Therefore, higher *MRC* values are achieved when *RH* of the air entering the DW (air state 1) are higher. The range of *MRC* values is $6.26 \text{ g} \cdot \text{kg}^{-1}$ – $10.56 \text{ g} \cdot \text{kg}^{-1}$ when ω_1 is $8 \text{ g} \cdot \text{kg}^{-1}$. While the range of *MRC* values is $11.52 \text{ g} \cdot \text{kg}^{-1}$ – $17.18 \text{ g} \cdot \text{kg}^{-1}$ when ω_1 is $14 \text{ g} \cdot \text{kg}^{-1}$. Therefore, the DW of the RACU shows higher *MRC* values for higher values of inlet air humidity.

According to the expression of Eq. (3), the range of the *KPI_{DW}* values is between $3.25 \text{ kg} \cdot \text{h}^{-1} \cdot \text{kW}^{-1}$ and $15.78 \text{ kg} \cdot \text{h}^{-1} \cdot \text{kW}^{-1}$ (Fig. 11). The \dot{W}_{PF} and \dot{W}_{RF} values ranged between 0.52 – 1.98 kW and 0.20 – 1.04 kW , respectively. The lowest *KPI_{DW}* value ($3.25 \text{ kg} \cdot \text{h}^{-1} \cdot \text{kW}^{-1}$) is shown for test N6, in which the ω_1 value is $11 \text{ g} \cdot \text{kg}^{-1}$ and the T_1 value is 40°C . However, the highest *KPI_{DW}* value ($15.78 \text{ kg} \cdot \text{h}^{-1} \cdot \text{kW}^{-1}$) is shown for test N18 which showed a high value of ω_1 ($14 \text{ g} \cdot \text{kg}^{-1}$) and the T_1 value is 32°C (Fig. 11). Therefore, higher *KPI_{DW}* values are also achieved for higher *RH* values of *Pi* air. The range of *KPI_{DW}* values is $3.50 \text{ kg} \cdot \text{h}^{-1} \cdot \text{kW}^{-1}$ – $8.41 \text{ kg} \cdot \text{h}^{-1} \cdot \text{kW}^{-1}$ when ω_1 is $8 \text{ g} \cdot \text{kg}^{-1}$. While the range of *KPI_{DW}* values is $5.79 \text{ kg} \cdot \text{h}^{-1} \cdot \text{kW}^{-1}$ – $15.78 \text{ kg} \cdot \text{h}^{-1} \cdot \text{kW}^{-1}$ when ω_1 is $14 \text{ g} \cdot \text{kg}^{-1}$. Therefore, higher *MRC* values due to higher values inlet air humidity ratio increased the *KPI_{DW}* value for DW in RACU. Higher *KPI_{DW}* values are also achieved when the electrical-power consumption of the process and regeneration fans are lower, as shown in Fig. 11.

The DIEC performance results in terms of ε_{DP} and KPI_{DIEC} are also analysed for all tests carried out at RACU (Fig. 12). According to the expression of Eq. (4), high values of ε_{DP} are shown for DIEC in this work. The range of the ε_{DP} values is between 0.59 and 0.96, as observed from Fig. 12. The lowest ε_{DP} value (0.59) is shown for test N59 and the highest ε_{DP} value (0.96) is shown for test N43. The DIEC inlet air temperature values (T_2) for both tests are similar (around 42°C). However, the DIEC inlet air humidity values (ω_2) are different: $5.41 \text{ g} \cdot \text{kg}^{-1}$ for test N59 and $10.61 \text{ g} \cdot \text{kg}^{-1}$ for test N43. Thus, higher ε_{DP} value for test N43 is shown due to the higher T_{DP} value than for test N59. The range of ε_{DP} values is 0.59–0.79 when ω_1 is $8 \text{ g} \cdot \text{kg}^{-1}$. However, the range of ε_{DP} values is

0.68–0.96 when ω_1 is $14 \text{ g} \cdot \text{kg}^{-1}$. Therefore, higher ε_{DP} values are also shown for higher ω_1 values, so higher ω_2 values, due to the higher $T_{DP,2}$ values. This can also be explained with the expression in Eq. (4).

According to the expression of Eq. (5), the range of the $\dot{Q}_{S,DIEC,U}$ values is between 7.59 – 21.49 kW , as shown in Fig. 12. The highest $\dot{Q}_{S,DIEC,U}$ value (21.49 kW) is shown for test N48, in which the T_2 value is 45.9°C and the ω_2 value is $7.91 \text{ g} \cdot \text{kg}^{-1}$. The lowest $\dot{Q}_{S,DIEC,U}$ value (7.59 kW) is shown for test N3, in which the T_2 value is 35.8°C and the ω_2 value is $8.97 \text{ g} \cdot \text{kg}^{-1}$. Thus, higher $\dot{Q}_{S,DIEC,U}$ values are achieved for higher T_2 values and lower ω_2 values, so when *RH* of the air entering the DIEC (air state 2) is lower. Also, according to Eq. (5), the *KPI_{DIEC}* values are between 10.06 and 42.81 (Fig. 12). The range of the \dot{W}_{DF} values is between 0.35 kW , for test N14, and 1.10 kW , for test N11. Higher \dot{W}_{DF} values are shown due to higher \dot{V}_{Po} values. It can be observed that the highest *KPI_{DIEC}* value (42.81) is shown for test N14, with the lowest \dot{W}_{DF} value, and the T_2 and ω_2 values of 47.3°C and $7.35 \text{ g} \cdot \text{kg}^{-1}$, respectively. However, the lowest *KPI_{DIEC}* value (10.06) is shown for test N11, with the highest \dot{W}_{DF} value, and the T_2 and ω_2 values of 41.8°C and $8.90 \text{ g} \cdot \text{kg}^{-1}$, respectively. The range of *KPI_{DIEC}* values is 11.50 – 34.52 when T_1 is 24°C . However, the range of *KPI_{DIEC}* values is 15.49 – 42.81 when T_1 is 40°C . Thus, higher *KPI_{DIEC}* values are also shown for higher inlet air temperatures, as well as when *RH* of the air entering the DIEC (air state 2) is lower. Lower \dot{W}_{DF} values due to lower \dot{V}_{Po} values also increase the *KPI_{DIEC}* values, as observed from Fig. 12.

3.2.4. Performance of renewable air-cooling unit under experimental test conditions

In this section, the percentage of $\dot{Q}_{S,DIEC,T}$ used to compensate for the $\dot{Q}_{S,DW}$ is evaluated for each experimental test, see the *HCP* values in Fig. 13. The $\dot{Q}_{S,DW}$ values are between 5.45 kW , for test N38, and 21.98 kW , for test N49 (Fig. 13). The conditions of the inlet air to DW (air state 1) are 40°C and $8 \text{ g} \cdot \text{kg}^{-1}$ for test N38, and 24°C and $11 \text{ g} \cdot \text{kg}^{-1}$, for test N49. Thus, higher $\dot{Q}_{S,DW}$ values are shown for higher RH values of the inlet air conditions to DW. The range of the $\dot{Q}_{S,DIEC,T}$ values is between 18.70 kW , for test N55, and 39.22 kW , for test N48 (Fig. 13). Regarding

Table 6

Correlation models and statistical parameters for RACU.

Estimated Parameters	Estimated Output value	T_{Po}	ω_{Po}	T_{Ro}	ω_{Ro}	COP	Input Variables
b_0	45.1267	9.8932	21.4788	36.9173	-8.2047	—	
b_1	-0.4784	-0.1640	0.5426	-1.2408	1.1708	T_{Pi}	
b_2	-0.6294	0.3084	-1.6944	1.1131	1.0662	ω_{Pi}	
b_3	0.0042	0.0007	0.0025	-0.0025	-0.0033	\dot{V}_{Pi}	
b_4	-63.2453	-15.1635	-7.0615	-4.0375	29.8432	R_e	
b_5	-0.7054	-0.2887	-0.2240	-0.3831	0.1504	T_{Ri}	
b_6	0.5269	0.8558	-0.9489	0.9049	-1.8444	ω_{Ri}	
b_7	-0.0067	-0.0066	0.0215	-0.0028	0.0011	\dot{V}_{Ri}	
b_8	0.03849	-0.0015	—	—	-0.0067	$T_{Pi} \cdot \omega_{Pi}$	
b_9	—	1.0417E-5	-8.2083E-5	0.0002	-7.8958E-5	$T_{Pi} \cdot \dot{V}_{Pi}$	
b_{10}	-0.2227	—	—	—	-0.5336	$T_{Pi} \cdot R_e$	
b_{11}	0.0119	—	-0.0045	0.0046	—	$T_{Pi} \cdot T_{Ri}$	
b_{12}	0.0170	-0.0068	0.0148	0.0428	0.0067	$T_{Pi} \cdot \omega_{Ri}$	
b_{13}	-0.0001	4.7500E-5	-0.0003	5.6875E-5	-9.9688E-5	$T_{Pi} \cdot \dot{V}_{Ri}$	
b_{14}	—	-2.5556E-5	-0.0002	—	-6.4444E-5	$\omega_{Pi} \cdot \dot{V}_{Pi}$	
b_{15}	—	0.2542	—	—	-0.3604	$\omega_{Pi} \cdot R_e$	
b_{16}	—	0.0104	0.0143	-0.0083	—	$\omega_{Pi} \cdot T_{Ri}$	
b_{17}	—	-0.0144	—	-0.0379	0.0221	$\omega_{Pi} \cdot \omega_{Ri}$	
b_{18}	—	-7.8333E-5	-0.0003	-0.0001	-0.0002	$\omega_{Pi} \cdot \dot{V}_{Ri}$	
b_{19}	0.0030	0.0005	—	—	0.0018	$\dot{V}_{Pi} \cdot R_e$	
b_{20}	—	-2.1667E-5	6.3333E-5	3.8958E-5	3.8750E-5	$\dot{V}_{Pi} \cdot T_{Ri}$	
b_{21}	—	—	0.0001	—	—	$\dot{V}_{Pi} \cdot \omega_{Ri}$	
b_{22}	9.9667E-7	2.2000E-7	-9.5333E-7	—	1.6867E-6	$\dot{V}_{Pi} \cdot \dot{V}_{Ri}$	
b_{23}	—	—	—	—	-0.1047	$T_{Ri} \cdot R_e$	
b_{24}	0.0296	0.0173	—	0.0327	-0.0092	$T_{Ri} \cdot \omega_{Ri}$	
b_{25}	—	-0.1458	—	—	0.5563	$\omega_{Ri} \cdot R_e$	
b_{26}	—	-0.0001	-0.0003	-0.0002	9.5833E-5	$\omega_{Ri} \cdot \dot{V}_{Ri}$	
b_{27}	0.0055	0.0020	—	—	—	$\dot{V}_{Ri} \cdot R_e$	
b_{28}	—	0.0027	0.0119	-0.0031	-0.0034	T_{Pi}^2	
b_{29}	—	0.0169	0.0819	—	-0.0194	ω_{Pi}^2	
b_{30}	-8.4833E-7	—	—	-5.3511E-7	—	\dot{V}_{Pi}^2	
b_{31}	37.1328	9.1594	8.1510	4.0375	-27.0016	R_e^2	
b_{32}	—	0.0010	—	-0.0033	-0.0022	T_{Ri}^2	
b_{33}	-0.0840	-0.0288	0.0391	-0.0862	0.0505	ω_{Ri}^2	
b_{34}	1.4812 E-6	1.5880E-6	—	1.216E-6	-1.7503E-6	\dot{V}_{Ri}^2	
R^2 [-]	0.9483	0.9738	0.9701	0.9006	0.9804		
Adj. R^2 [-]	0.9276	0.9542	0.9551	0.8475	0.9658		
Std. dev. [-]	0.5141	0.0407	0.3598	0.5817	0.1666		
MAE [-]	0.4558	0.1805	0.5218	0.4376	0.2407		

the conditions of the inlet air to DIEC (air state 2), the RH value for test N48 is lower than for test N55 due to the higher T_2 value and the lower ω_2 value. Therefore, higher $\dot{Q}_{S,DIEC,T}$ values are achieved for lower RH_2 values. According to Eq. (6), the range of HCP values for RACU is between 16.80 % and 92.92 %, as observed from Fig. 13. The lowest HCP value (16.80 %) is shown for test N38, with the lowest $\dot{Q}_{S,DW}$ value (5.45 kW), as shown in Fig. 13. The highest HCP value (92.92 %) is shown for test N57, which showed the same T_1 and ω_1 values as test N49 (with the highest $\dot{Q}_{S,DW}$ value) and air state 2 conditions very similar to those of test N57 (with the lowest $\dot{Q}_{S,DIEC,T}$ value), as observed from Fig. 13. Thus, it can be observed that higher HCP values are also shown for higher RH values of the inlet air to DW (air state 1), due to the higher dehumidification capacity.

The RACU performance results in terms of $\dot{Q}_{S,RACU}$, $\dot{Q}_{L,RACU}$, \dot{W}_{elect} and COP are also obtained for all experimental tests, as observed from Fig. 14. According to the expression in Eq. (7), the range of the $\dot{Q}_{S,RACU}$ values is between 1.86–16.43 kW. The lowest $\dot{Q}_{S,RACU}$ value (1.86 kW) is shown for test N57, which showed the highest HCP value (92.92 %) and the lowest T_1 value (24 °C). However, the highest $\dot{Q}_{S,RACU}$ value (16.43 kW) is shown for test N48, with the same ω_1 value as test N57 and the highest T_1 value (40 °C). The \dot{V}_{Po} values in tests N57 and N48 are similar. Therefore, higher $\dot{Q}_{S,RACU}$ values are achieved when the HCP values are lower, so less need to dehumidify the air entering the RACU. The RACU prototype also achieved higher $\dot{Q}_{S,RACU}$ values when T_1 are

higher, due to its higher sensible cooling capacity (Fig. 14).

According to the expression of Eq. (8), the range of the $\dot{Q}_{L,RACU}$ values is between 1.57–8.86 kW. The lowest $\dot{Q}_{L,RACU}$ value (1.57 kW) is shown for test N9, with the T_1 value of 32 °C, but the lowest ω_1 value (8 g·kg⁻¹), so lower dehumidification capacity of RACU. However, the highest $\dot{Q}_{L,RACU}$ value (8.86 kW) is shown for test N60, with the same T_1 value as test N9, but the highest ω_1 value (14 g·kg⁻¹), so higher dehumidification capacity of RACU (Fig. 14). Thus, higher $\dot{Q}_{L,RACU}$ values are achieved when the ω_1 values are higher, so higher values of MRC.

The range of the \dot{W}_{elect} values for RACU is between 1.08–3.72 kW, according to the expression of Eq. (9). Since the electrical-power consumption values of the DW drive motor and the internal HP in DIEC are very lower compared to the electrical-power consumption of the fans, \dot{W}_{elect} depended mainly on the volumetric airflow rates. The lowest \dot{W}_{elect} value (1.08 kW) is shown for test N18, in which the \dot{V}_{Pi} and \dot{V}_{Ri} values are the minimum values of their DOE ranges, see Table 5. The highest \dot{W}_{elect} value (3.72 kW) is shown for test N54, in which the \dot{V}_{Pi} and \dot{V}_{Ri} values had the maximum DOE values. Therefore, higher \dot{W}_{elect} values for RACU are shown for higher \dot{V}_{Pi} and \dot{V}_{Ri} values.

The COP values for RACU are obtained according to Eq. (10) to evaluate the overall energy performance of this hybrid air-cooling prototype, including the sensible cooling and the latent capacity of RACU. The experimental results in this work showed high COP values for RACU, from 1.77 to 11.00, as seen in Fig. 14. The highest COP value (11.00) is achieved for test N14, with the highest value of T_1 (40 °C). For

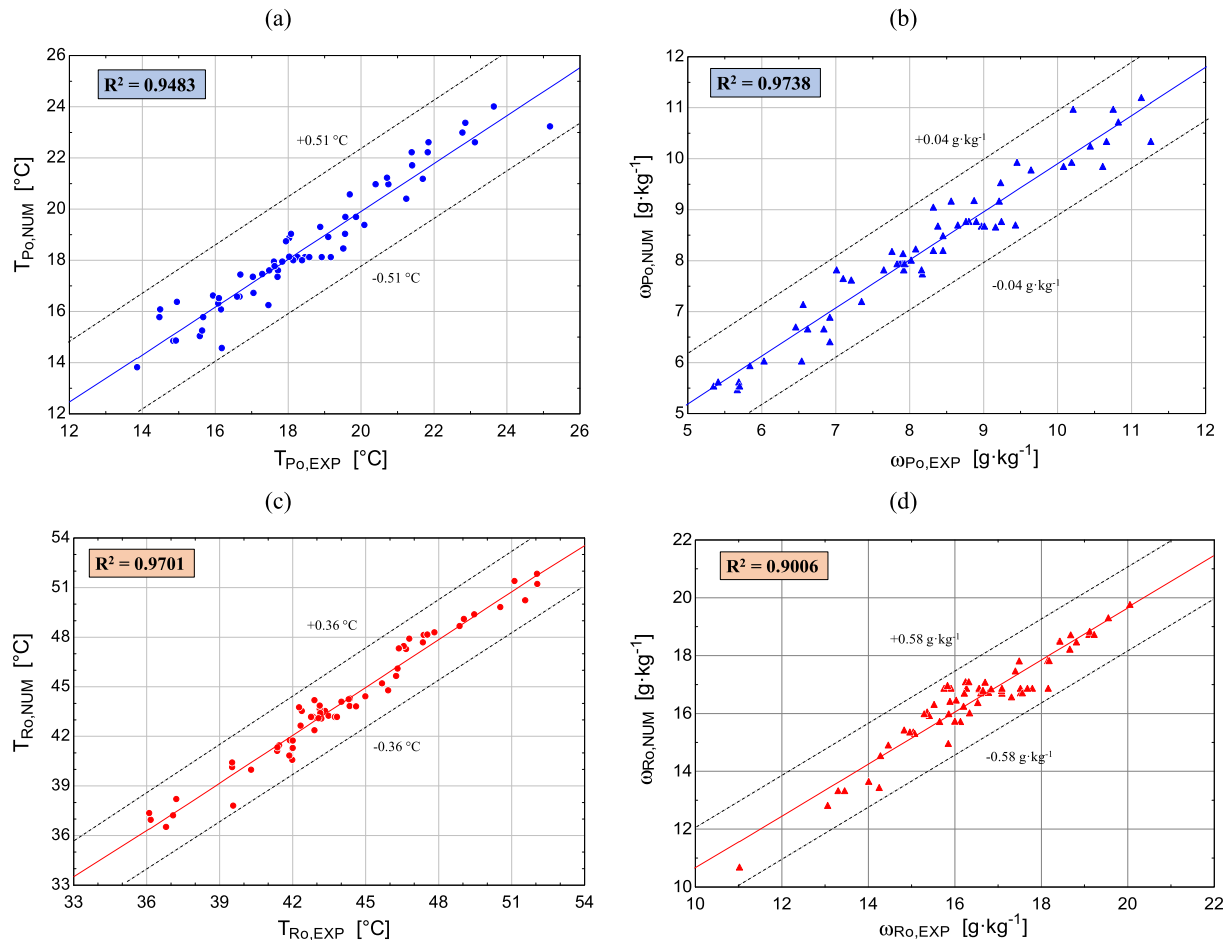


Fig. 10. Parity plot of experimental and numerical results for: (a) T_{Po} ; (b) ω_{Po} ; (c) T_{Ro} ; (d) ω_{Ro} .

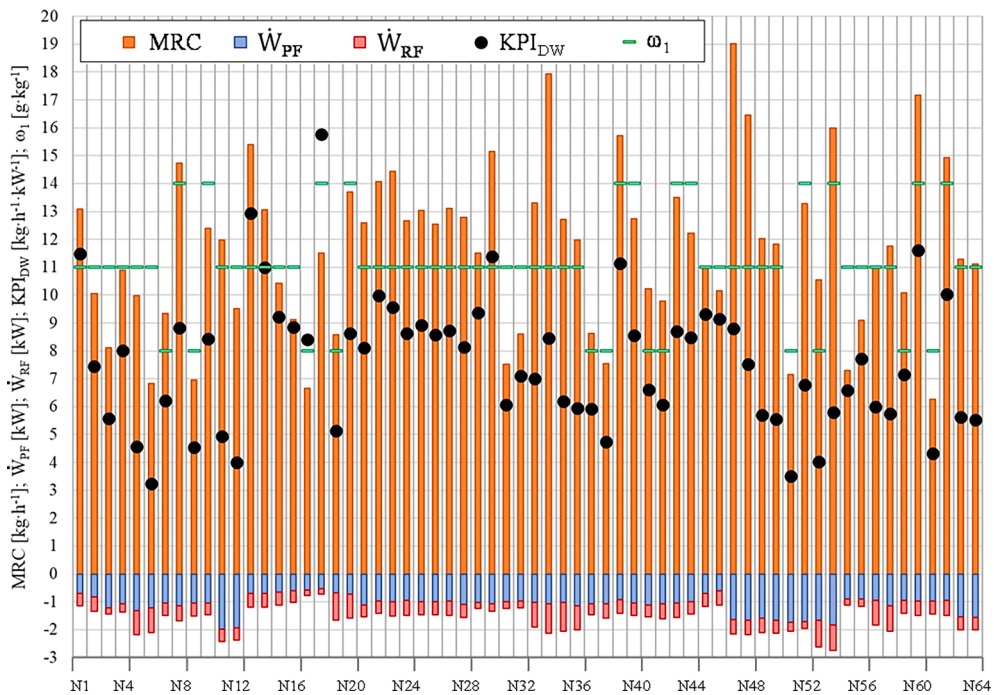


Fig. 11. Values of MRC and KPI_{DW} for tests N1-N64.

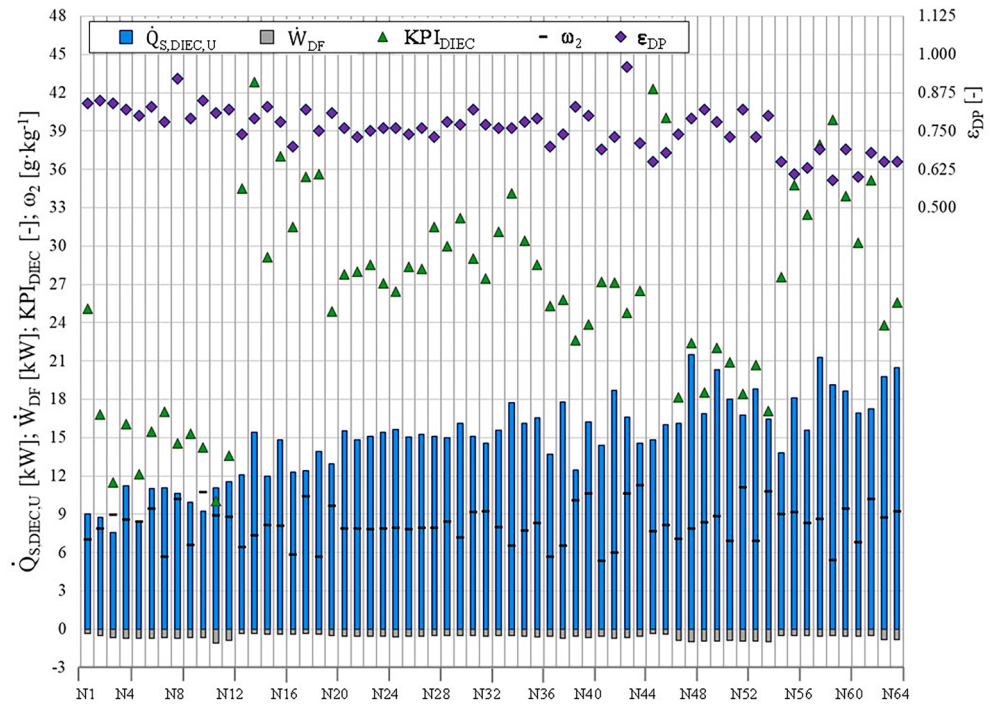
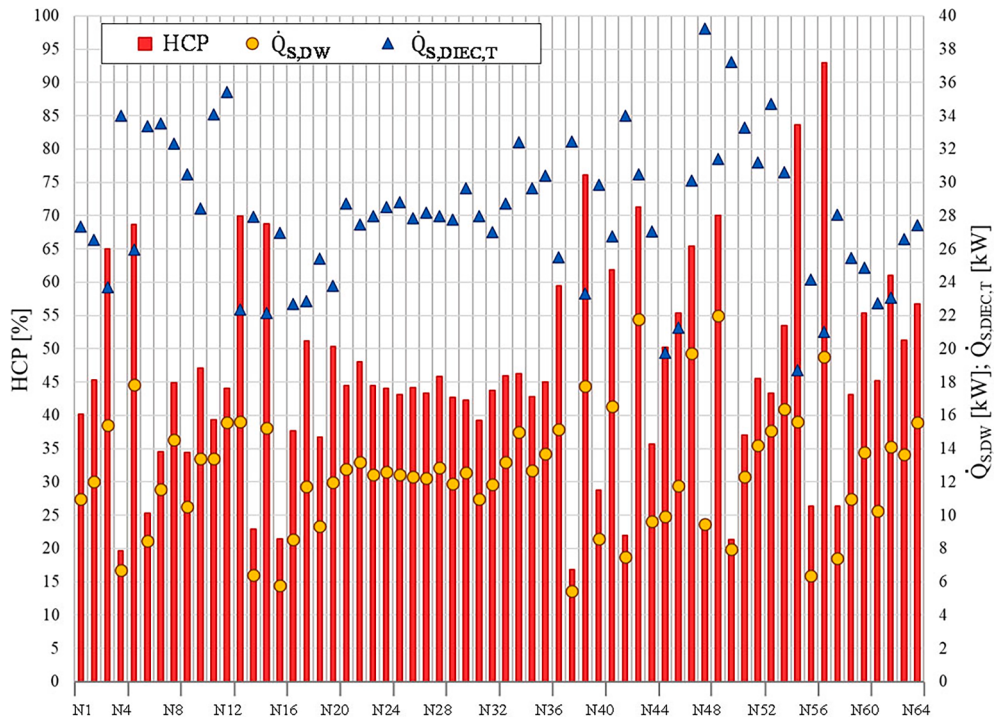
Fig. 12. Values of ϵ_{DP} and KPI_{DIEC} for tests N1-N64.

Fig. 13. Values of HCP for tests N1-N64.

this test N14 the KPI_{DIEC} index had the highest value (42.81) and the \dot{W}_{elect} value (1.55 kW) is close to the lowest \dot{W}_{elect} value. However, the lowest COP value (1.77) is obtained for test N5, in which \dot{W}_{elect} showed a high value (2.87 kW). The ω_1 value in test N5 ($11 \text{ g}\cdot\text{kg}^{-1}$) is the same as that in test N14. The $\dot{Q}_{S,RACU}$ value for test N5 is low (2.90 kW) due to the low value of T_1 (24°C). Therefore, it can be observed that, for similar air flow rates, the energy performance for RACU increases when the inlet air conditions become more severe (high T_{pi} and ω_{pi} values), a contrast

to traditional air-cooling systems. However, influence of \dot{V}_{pi} and \dot{V}_{Ri} caused the opposite effect: an increase in the \dot{V}_{pi} and \dot{V}_{Ri} values resulted in a decrease in the COP value for RACU, mainly due to the increase in electrical-power consumption of the fans.

These experimental results obtained for the RACU system have been compared with the results for other hybrid air cooling systems. A maximum COP value of 3.5 was obtained for an air-cooling system composed of a DW and an evaporative cooler, under the severe climatic

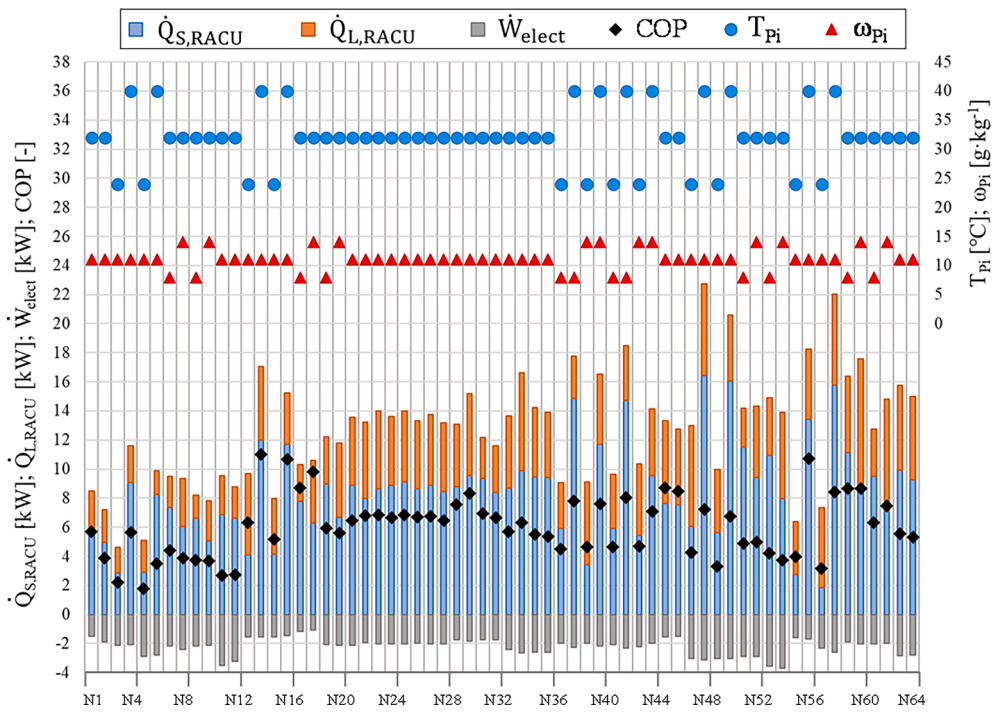


Fig. 14. Experimental results of $\dot{Q}_{S,RACU}$, $\dot{Q}_{L,RACU}$, \dot{W}_{elect} and COP for the tests N1-N64.

conditions of Iran [25]. In another simulation work, the authors obtained energy efficiency ratio (*EER*) values of up to 30 depending on the type of hybrid system, consisting of two evaporative coolers and a DW [26]. A desiccant DIEC showed an *EER* value of 5 for T_{Pi} of 40°C and ω_{Pi} of $10 \text{ g} \cdot \text{kg}^{-1}$ in a recent experimental work [27]. For these same air conditions RACU presented a maximum *COP* value of 11.0, as observed from Fig. 14.

4. Conclusions

In the present work, an experimental evaluation of a novel renewable air-cooling unit is developed. This air-cooling system prototype is based on a DIEC and a DW. An extensive number of experimental tests (N1–N64) is carried out according to the statistical technique of DOE. Several correlation models are adjusted according to the output variables T_{Po} , ω_{Po} , T_{Ro} , ω_{Ro} and *COP* for RACU. In addition, several performance indices for DW and DIEC are developed. Therefore, the main conclusions of this experimental work are:

- DW performance indices: Higher values of MRC , up to $19.02 \text{ kg} \cdot \text{h}^{-1}$, are achieved for higher RH values of the air entering the DW. The KPI_{DW} values are also higher when these RH values are higher, and for lower \dot{V}_{Pi} and \dot{V}_{Ri} values, so lower \dot{W}_{PF} and \dot{W}_{RF} values.
- DIEC performance indices: Higher values of ϵ_{DP} , up to 0.96, are achieved for higher T and ω values of the air entering the DIEC, due to the higher $\dot{Q}_{S,DIEC,U}$ and $T_{DP,2}$ values, respectively. In addition, higher KPI_{DIEC} values, up to 42.81, are shown for lower RH values of the air entering the DIEC and for lower \dot{V}_{Pi} values, so lower \dot{W}_{DF} values.
- RACU performance: The energy performance of RACU is obtained based on its sensible cooling capacity and latent capacity, reaching high *COP* values, up to 11.0. This *COP* value increased when the inlet air conditions become more severe (high T_{Pi} and ω_{Pi} values), in contrast to traditional air-cooling systems. The *COP* values for RACU decreased when the \dot{V}_{Pi} and \dot{V}_{Ri} increased, so higher fans electrical-power consumption.

The obtained findings can guide future studies focusing on the energy performance analysis of advanced efficient air-cooling systems for buildings in sustainable environments. The empirical correlation models of the RACU prototype, with high values of R^2 , could be useful for different applications in the building environment. In addition, RACU independent control of air temperature, air humidity and carbon dioxide level offers an opportunity for improving energy efficiency, thermal comfort, and indoor air quality in buildings. A valuable target of this hybrid air-cooling system under heat waves and the climate change world scenario.

Authors contributions

M.J.R.-L. carried out the experimental tests and wrote the manuscript; F.C. discussed the results and carried out several revisions of the manuscript; M.R.d.A. conceptualized the idea of the performance indices, discussed the results, and carried out several revisions of the manuscript.

CRedit authorship contribution statement

Maria Jesus Romero-Lara: Writing – original draft, Investigation, Formal analysis, Data curation. **Francisco Comino:** Writing – review & editing, Supervision, Investigation, Formal analysis. **Manuel Ruiz de Adana:** Writing – review & editing, Supervision, Investigation, Funding acquisition, Formal analysis.

Declaration of competing interest

The authors declare that they have no known competing financial interests or personal relationships that could have appeared to influence the work reported in this paper.

Data availability

Data will be made available on request.

Acknowledgments

The authors acknowledge the financial support received by European Union's Horizon 2020 research and innovation programme, through the research project WEDISTRICT, reference H2020-WIDESPREAD2018-03-857801, and by the DCOOL project, reference TED2021-129648B-I00, funded by MCIN/AEI/10.13039/501100011033 and the European Union "NextGenerationEU/PRTR". Funding for open access charge: Universidad de Córdoba / CBUA.

References

- [1] Energy, Climate change, Environment. Heat pumps. Official website of the European Union. [Online]. Available: https://energy.ec.europa.eu/topics/energy-efficiency/heat-pumps_en.
- [2] Ciancio V, Salata F, Falasca S, Curci G, Golasi I, de Wilde P. Energy demands of buildings in the framework of climate change: An investigation across Europe. *Sustain Cities Soc* 2020;60:102213.
- [3] Pörtner HO, Roberts DC, Adams H, Adler C, Aldunce P, Ali E. Climate Change 2022: Impacts, Adaptation and Vulnerability. Intergovernmental Panel on Climate Change, pp. 7–12, 2022.
- [4] Romero-Lara MJ, Comino F, Ruiz de Adana M. Seasonal Analysis Comparison of Three Air-Cooling Systems in Terms of Thermal Comfort, Air Quality and Energy Consumption for School Buildings in Mediterranean Climates. *Energies* 2021;14 (15):4436.
- [5] Jani DB, Mishra M, Sahoo PK. Solid desiccant air conditioning - A state of the art review. *Renew Sustain Energy Rev* 2016;60:1451–69.
- [6] Comino F, Ruiz de Adana M, Peci F. Energy saving potential of a hybrid HVAC system with a desiccant wheel activated at low temperatures and an indirect evaporative cooler in handling air in buildings with high latent loads. *Appl Therm Eng* 2018;131:412–27.
- [7] Pandelidis D, Anisimov S, Worek WM, Dra P. Comparison of desiccant air conditioning systems with different indirect evaporative air coolers. *Energy Convers Manag* 2016;117:375–92.
- [8] Güzelel YE, Olmus U, Büyükkalaca O. Simulation of a desiccant air-conditioning system integrated with dew-point indirect evaporative cooler for a school building. *Appl Therm Eng* 2022;217.
- [9] Romero-Lara MJ, Comino F, Ruiz de Adana M. Seasonal energy efficiency ratio of regenerative indirect evaporative coolers—Simplified calculation method. *Appl Therm Eng* 2022;220:119710.
- [10] Lin J, Huang S, Wang R, Jon K. Thermodynamic analysis of a hybrid membrane liquid desiccant dehumidification and dew point evaporative cooling system. *Energy Convers Manag* 2018;156:440–58.
- [11] Comino F, Guijo-Rubio D, Ruiz de Adana M, Hervás-Martínez C. Validation of multitask artificial neural networks to model desiccant wheels activated at low temperature. *Int J Refrig* 2019;100:434–42.
- [12] Comino F, Ruiz de Adana M. Experimental and numerical analysis of desiccant wheels activated at low temperatures. *Energy Build* 2016;133:529–40.
- [13] Liang J, Kao C, Tsai L, Chiang Y, Tsai H, Chen S. Performance investigation of a hybrid ground-assisted desiccant cooling system. *Energy Convers Manag* 2022;265: 115765.
- [14] Comino F, Castillo González J, Navas-Martos FJ, Ruiz de Adana M. Experimental energy performance assessment of a solar desiccant cooling system in Southern Europe climates. *Appl Therm Eng* 2020;165:114579.
- [15] Chun L, Gong G, Peng P, Wan Y, Chua KJ, Fang X, Li W. Research on thermodynamic performance of a novel building cooling system integrating dew point evaporative cooling, air-carrying energy radiant air conditioning and vacuum membrane-based dehumidification (DAV-cooling system). *Energy Convers. Manag.*, vol. 245, 2021.
- [16] EnergyPlus software v23.2.0. <https://energyplus.net/>.
- [17] Klein SA. TRNSYS 17: A Transient System Simulation Program. Madison USA, SEL: University of Wisconsin; 2006.
- [18] Castillo-González J, Comino F, Navas-Martos FJ, M. Ruiz de Adana M. Life cycle assessment of an experimental solar HVAC system and a conventional HVAC system. *Energy Build.*, vol. 256, 2022.
- [19] Kulkuş Ş, Krajačić G, Duif N, Rosen MA, Al-Nimr MA. Sustainable development of energy, water and environment systems in the critical decade for climate action. *Energy Convers. Manag.*, vol. 296, 2023.
- [20] Wedistrict project. European Union's Horizon 2020 research and innovation programme. Grant agreement N°85780.
- [21] Comino F, Romero-Lara MJ, Ruiz de Adana M. Experimental and numerical study of dew-point indirect evaporative coolers to optimize performance and design. *Int J Refrig* 2022;142:92–102.
- [22] Montgomery DC. Design and Analysis of Experiments. Ninth 2004.
- [23] Statgraphics Centurion XV. 2006. [Online]. Available: <http://www.statgraphics.com/>. [Accessed: 02-Dec-2022].
- [24] JCGM (Working Group 1). Joint Committee for Guides in Metrology. JCGM 100. Evaluation of measurement data – Guide to the expression of uncertainty in measurement. Int. Organ. Stand. Geneva ISBN, vol. 50, p. 134, 2008.
- [25] Heidari A, Roshandel R, Vakiloroaya V. An innovative solar assisted desiccant-based evaporative cooling system for co-production of water and cooling in hot and humid climates. *Energy Convers Manag* 2019;185:396–409.
- [26] Pandelidis D, Pacak A, Cichon A, Drag P, Worek W, Cetin S. Numerical and experimental analysis of precooled desiccant system. *Appl Therm Eng* 2020;181: 115929.
- [27] Mumtaz M, Pamintuan BC, Fix AJ, Braun JE, Warsinger DM. Hybrid membrane dehumidification and dewpoint evaporative cooling for sustainable air conditioning. *Energy Convers Manag* 2023;294:117547.